

Numerical Studies of Axial and Radial Magnetic Forces Between High Temperature Superconductors and a Magnetic Rotor

Guangtong Ma · Qunxu Lin · Donghui Jiang ·
Chunyan Yuan · Zigang Deng

Received: 23 December 2012 / Accepted: 6 March 2013 / Published online: 21 March 2013
© Springer Science+Business Media New York 2013

Abstract The magnetic bearing is considered as one of the most prospective applications of high temperature superconductors (HTSs) which can realize stable levitation in a magnetic field generated by permanent magnet devices or coils. The exploration of this kind of HTS bearing through numerical investigation is usually made by assuming the induced current circulates only within the *ab*-plane and thus simplifying the actual three-dimensional problem to a two-dimensional one. In this paper, on the basis of the three-dimensional model of the HTS bulk established before, we further introduce the developed finite-element software to calculate the magnetic field generated by a magnetic rotor which is composed of permanent magnet (PM) rings and ferromagnet (FM) shims, and in this way, we can investigate the magnetic forces (radial force and axial force) of a simplified HTS bearing model, i.e., two symmetric HTS bulks and a magnetic rotor, at a three-dimensional level. The investigations performed in this paper lead to the observations: the favorable configuration to construct the HTS bearing is that the axial height of each HTS element should be equivalent to the axial heights of PM ring plus FM shim; the increase of the radial thickness of PM ring will improve both the radial force and the axial force considerably, but its margin decreases; the enhancement of critical current density of HTSs due to the decrease of operating temperature can result in a higher increase of both the radial and axial force with a lower nominal gap between the HTSs and the magnetic rotor.

G. Ma (✉) · Q. Lin · D. Jiang · Z. Deng
Applied Superconductivity Laboratory, State Key Laboratory of Traction Power, Southwest Jiaotong University, Chengdu, Sichuan 610031, China
e-mail: gma@home.swjtu.edu.cn

Q. Lin
e-mail: linkqunxu@gmail.com

C. Yuan
Institute of Plasma Physics, Chinese Academy of Sciences, Hefei, Anhui 230031, China

Keywords High temperature superconductors · Magnetic levitation · Magnetic bearing · Magnetic rotor · Magnetic forces

1 Introduction

As one of the most prospective applications of the stable levitation technology using the high temperature superconductors (HTSs), the HTS bearing has been investigated intensively in both experiment [1–7] and theory [6–11] and towards to practical demonstration [12–15]. From a theoretical point of view, most effort was made by assuming the induced current circulates only within the ab -plane and thus simplifying the actual three-dimensional problem to be a two-dimensional one [6–11]. This assumption and simplification is reasonable for the case of a symmetrical configuration without radial displacement like the traditional journal magnetic bearing model with a cylindrical HTS bulk above a cylindrical permanent magnet (PM), since the induced current in the HTS bulk of this case only flow within the ab -plane. However, the HTS bulks in the more favorable configuration of radial bearing are exposed to a more complicated magnetic field, and the induced current in the HTS bulks not only flow within the ab -plane but also along the c -axis. Therefore, the full three-dimensional model is required for providing better numerical results for practical design of the radial bearing.

Using the previously established three-dimensional finite-element environment for investigating the levitation performance of a HTS bulk above a permanent magnet guideway [16] and combining this environment with the developed finite-element software which is used to calculate the magnetic field of the magnetic rotor made of the PM rings and the ferromagnet (FM) shims, we programmed a updated finite-element environment that can estimate the radial force as well as the axial force between the HTS bulks and the magnetic rotor. Some preliminary results, concerning the configuration of the HTS bulk relative to the magnetic rotor, the geometrical parameters of the PM ring and the FM shim as well as the operating temperature, obtained by this updated finite-element environment will be reported in this paper.

2 Numerical Model

2.1 Mathematical Foundations

A finite-element program based on our previous work was updated to investigate the radial force and the axial force between the HTS bulks and the magnetic rotor. The partial differential equations (PDEs) for governing the electromagnetic properties of HTS in three dimensional cases were established by using the current vector potential (T_x , T_y and T_z) as the state variable and the anisotropic feature of the HTS was considered in the electromagnetic governing equations by introducing a tensor resistivity [16].

$$\begin{aligned} & \frac{1}{\sigma_{ab}} \left(-\frac{\partial^2 T_x}{\partial x^2} - \alpha \frac{\partial^2 T_x}{\partial y^2} - \frac{\partial^2 T_x}{\partial z^2} + (\alpha - 1) \frac{\partial^2 T_y}{\partial x \partial y} \right) + \mu_0 C(P) \frac{\partial T_x}{\partial t} \\ & + \frac{\mu_0}{4\pi} \int_S \frac{\partial(\mathbf{n}' \cdot \mathbf{T}')}{\partial t} \frac{\partial}{\partial x'} \left(\frac{1}{R(P, P')} \right) dS' + \frac{\partial B_{ex}}{\partial t} = 0 \end{aligned} \tag{1}$$

$$\begin{aligned} & \frac{1}{\sigma_{ab}} \left(-\alpha \frac{\partial^2 T_y}{\partial x^2} - \frac{\partial^2 T_y}{\partial y^2} - \frac{\partial^2 T_y}{\partial z^2} + (\alpha - 1) \frac{\partial^2 T_x}{\partial x \partial y} \right) + \mu_0 C(P) \frac{\partial T_y}{\partial t} \\ & + \frac{\mu_0}{4\pi} \int_S \frac{\partial(\mathbf{n}' \cdot \mathbf{T}')}{\partial t} \frac{\partial}{\partial y'} \left(\frac{1}{R(P, P')} \right) dS' + \frac{\partial B_{ey}}{\partial t} = 0 \end{aligned} \tag{2}$$

$$\begin{aligned} & \frac{1}{\sigma_{ab}} \left(-\frac{\partial^2 T_z}{\partial x^2} - \frac{\partial^2 T_z}{\partial y^2} - \frac{\partial^2 T_z}{\partial z^2} \right) + \mu_0 C(P) \frac{\partial T_z}{\partial t} \\ & + \frac{\mu_0}{4\pi} \int_S \frac{\partial(\mathbf{n}' \cdot \mathbf{T}')}{\partial t} \frac{\partial}{\partial z'} \left(\frac{1}{R(P, P')} \right) dS' + \frac{\partial B_{ez}}{\partial t} = 0. \end{aligned} \tag{3}$$

It is worth noting that a linear B – H constitutive relation, i.e. $\mathbf{B} = \mu_0 \mathbf{H}$, was assumed in deducing the above PDEs. The specification of the parameters in the above equations is: μ_0 is the permeability of vacuum; σ_{ab} is the conductivity in the ab -plane of the HTS; α is the anisotropic ratio between ab -plane and c -axis to consider the anisotropic behavior of the HTS in the governing equations; B_{ex} , B_{ey} , and B_{ez} are the three components of the external provided by magnetic rotor, respectively; $R(P, P')$ is the distance between the source point P' and the field point P , superscript $'$ refers to the quantity at source point, \mathbf{n}' is a unit vector out of the surface S' . The principle to determine the value of $C(P)$ in different domains is: $C(P) = 1$ when the point P is in the HTS but not on the surface S' ; when on the surface S' , $C(P) = 0.5$; otherwise, $C(P) = 0$.

When an index n is introduced and defined as $n = U_0/k\Theta$ where U_0 is the pinning potential of the superconductor at an absolute temperature Θ and k is the Boltzmann constant, the power law model used to describe the constitutive law between the electric field E and the current density j is expressed as:

$$\mathbf{E} = E_c \left(\frac{|\mathbf{j}|}{j_c} \right)^n \frac{\mathbf{j}}{|\mathbf{j}|} \tag{4}$$

where $E_c = 10^{-4}$ V/m is the critical electric field to determine the critical current density j_c .

To numerically solve the above-mentioned PDEs, the finite-element technique via Galerkin’s method and the finite-difference technique via Crank-Nicolson- θ method were successively applied to discretize (1) to (3) in the spatial and temporal domain. After the numerical treatment, the nonlinear system of finite-element equation to solve at n th time step can be expressed as an integrated matrix [16]:

$$\begin{aligned} & \left(\frac{[\mathbf{Q}]}{\Delta t} + \theta[\mathbf{K}(\sigma_{ab})] \right) \{T^n\} \\ & = \theta \{L^n\} + (1 - \theta) \{L^{n-1}\} + \left(\frac{[\mathbf{Q}]}{\Delta t} - (1 - \theta)[\mathbf{K}(\sigma_{ab})] \right) \{T^{n-1}\}. \end{aligned} \tag{5}$$

where $[\mathbf{K}(\sigma_{ab})]$ is a conductivity-dependent matrix and related with the coefficients of the first term of the left side of (1) to (3); $[\mathbf{Q}]$ is also a matrix and relative to the coefficients of the middle two terms of the left side of (1) to (3); $\{\mathbf{L}\}$ is a column vector and relevant to last term of the left side of (1) to (3); Δt represents the time interval between the adjacent time step. The parameter θ is adopted to be $2/3$ in the following calculations.

The numerical solution method and numerical procedure to implement (5) has been illuminated at length in [16], and it is not repeated here for concision.

Differing from our previous work with analytic method to calculate the magnetic field generated by the PM [17], we use the developed finite-element software to simulate the magnetic field, which, in our present work, is generated by the magnetic rotor. The basic reason for this improvement is that, for the magnetic bearing condition, the nominal gap between the HTS and the magnetic rotor is usually very small and the influence of the FM shim on the magnetic field distribution where the HTS is located cannot be neglected.

To simplify the calculation, considering that the induced field generated by the induced current in the HTS is much weaker than the applied field from the magnetic rotor, we ignore the influence of this induced field on the magnetic response of the FM shim in the magnetic rotor. This assumption makes it possible to solve the magnetic field of the magnetic rotor separately from the HTS, and remarkably reduces the complexity of the problem. We firstly define the geometrical model and associated parameters for the magnetic rotor in the developed finite-element software, and after this magnetic rotor is solved, the magnetic field file for this magnetic rotor will be transferred to our home-made program to generate the magnetic excitation information required in solving the electromagnetic governing equations of the HTS.

2.2 Proposed Configurations

As the radial magnetic bearing shows a better performance than its counterpart of journal one [13], we merely consider the radial force and the axial force of a radial magnetic bearing composed of the HTS bulks and magnetic rotor. For the real configuration of a radial HTS bearing, it usually consists of a magnetic rotor and a HTS stator made of several HTS bulks [3, 15]. Since this real geometry requires very long computational time, especially for the 3-D investigation (such as several days estimated in [18]), we simplified the radial bearing as two symmetric HTS bulks and a magnetic rotor, as shown in Fig. 1(a), to give some fundamental results about how the working conditions and geometrical parameters affect the magnetic forces exerting on the HTS bulks.

Three different configurations given respectively in Fig. 1(b)–(d), according to the relative position between the HTS bulks and the magnetic rotor, were proposed for the purpose of clarifying which has the best performance for use concerning the radial force and the axial force. For the configuration of Type I in Fig. 1(b), the axial height of HTS is twice as high as the axial height of the PM ring plus the axial height of the FM shim. For the configuration of Type II in Fig. 1(c) and of Type III in Fig. 1(d), the axial height of HTS is both equal to the axial height of the PM ring plus the axial height of the FM shim, but with different relative position to the magnetic rotor. For

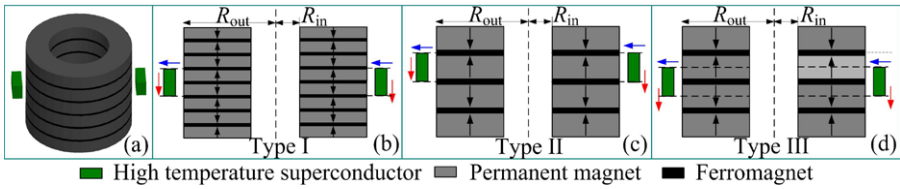


Fig. 1 The three- and two-dimensional views of the considered magnetic interaction system composed of two symmetric high temperature superconductors and a magnetic rotor constructed periodically with permanent magnet rings and ferromagnet shims. Three different configurations were considered, i.e., the configuration of type I illustrated in (b), the configuration of type II illustrated in (c), and the configuration of type III illustrated in (d) (Color figure online)

all configurations, the edge lines of the HTS bulks is in line with either the middle line of the PM ring or the middle line of the FM shim.

2.3 Specifications and Conditions Used for Investigation

In the following calculations, the parameters of the HTS bulk is kept constant. The index n for power law is of ~ 15 with the value of $U_0 = 0.1$ eV at 77.3 K. Its critical current density at liquid nitrogen (77.3 K) within the ab -plane $j_{c,ab}$ is 3.0×10^8 A/m², and along the c -axis $j_{c,c}$ is 1.0×10^8 A/m², indicating that an anisotropic ratio of 3 is presumed at 77.3 K according to the experimental observation on a melt-processed-single-domain Y–Ba–Cu–O by Murakami et al. [19]. The anisotropic effect of critical current density on the current flows along three axes has been estimated and displayed in our previous work concerning a HTS bulk above a permanent magnet guideway in [20]. Its geometry is 13 mm in radial thickness, 21 mm in axial height and 32 mm in width (direction perpendicular to the paper for Fig. 1(b)–(d)). The power law with its index $n = 15$ at liquid nitrogen is used to describe the nonlinear feature between the electric field E and the current density j in the HTS.

The PM ring used to assemble the magnetic rotor has a remanent magnetism B_r of 1.23 T and a coercivity of 8.9×10^5 A/m. In the default case, the PM ring has a dimension of 7.5 mm in the axial height for the configurations of Type I, and of 18 mm in the axial height for the configurations of Type II and Type III, and of 70 mm in the outer radius R_{out} and 40 mm in the inner radius R_{in} for all configurations. The FM shim of the magnetic rotor has a default axial height of 3 mm and the same default R_{out} and R_{in} as the PM ring. Material Steel1008 was appointed to the FM shim of the magnetic rotor. The FM shims in the magnetic rotor serve as the flux collectors to concentrate the magnetic field provided by the PM rings, as illustrated in details in [15].

The radial force during the radial movement and the axial force during the axial movement, are investigated on the basis of the above-mentioned parameters. For the case of axial movement, since the two symmetric HTS bulks illustrated in Fig. 1 are exposed to the same condition, only one of them is investigated and therefore the axial force given below is actually for one HTS bulk. For the case of radial movement, since the two symmetric HTS bulks illustrated in Fig. 1 are exposed to different conditions, i.e., one approaches to the magnetic rotor while the other departs from the magnetic

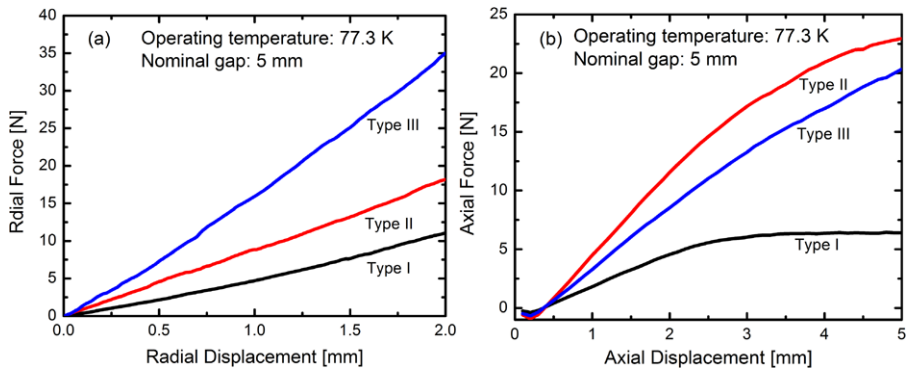


Fig. 2 The radial force (a) and the axial force (b) exerting on the high temperature superconductor for the three different configurations illustrated in Fig. 1. The maximum radial displacement for (a) is of 2.0 mm and the maximum axial displacement for (b) is of 5.0 mm. The nominal gap is of 5.0 mm for both the radial and axial movement (Color figure online)

rotor, both of them are investigated and therefore the radial force given below is actually for two HTS bulks.

3 Numerical Results and Discussion

3.1 The Radial/Axial Force with Different Configurations

We firstly investigate which kind of configuration illustrated in Fig. 1 has the best performance for generating the radial force as well as the axial force. We assume the HTS bulk is immersed in liquid nitrogen and has a 5 mm nominal gap to the magnetic rotor. The radial force exerting on the HTS bulks during the radial movement is plotted in Fig. 2(a). This figure clearly shows that, the configuration of Type III exhibits the highest radial force in the process of radial movement up to 2.0 mm. The axial force exerting on the HTS bulk during the axial movement is plotted in Fig. 2(b). This figure indicates that, the configuration of Type II can provide the highest axial force in the process of axial movement up to 5.0 mm. Through the further observation of Fig. 2, one can find that, the configuration of Type III can supply a radial force at the radial displacement of 2.0 mm around twice as high as that of the configuration of Type II, with a slightly lower axial force than the configuration of Type II. Therefore, from the overall view of both the radial and axial force, the configuration of Type III exhibits the best optimum performance. We thus use this configuration for the following investigation.

3.2 The Radial/Axial Force with Different Axial Heights of the FM Shim

With the other parameters defined as the default value and a nominal gap of 5.0 mm, we only alter the axial height of the FM shim and investigate how the radial force at the radial displacement of 2.0 mm and the axial force at the axial displacement of 5.0 mm vary with this geometrical parameter. From the bar charts shown in Fig. 3, one

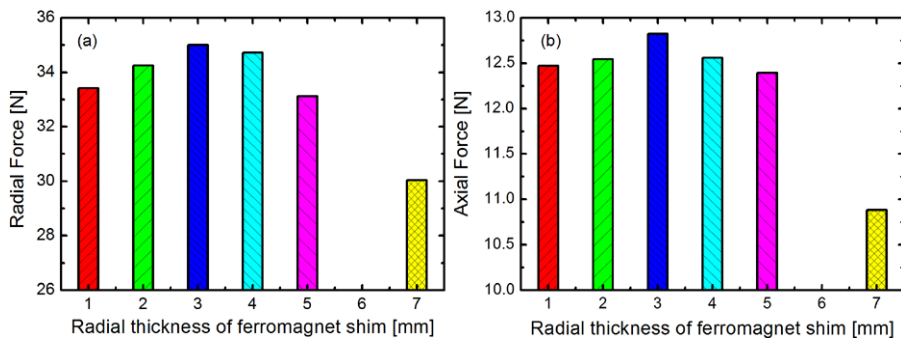


Fig. 3 The dependence of the radial force (a) and the axial force (b) on the axial height of the ferromagnet shims used to assemble the magnetic rotor (Color figure online)

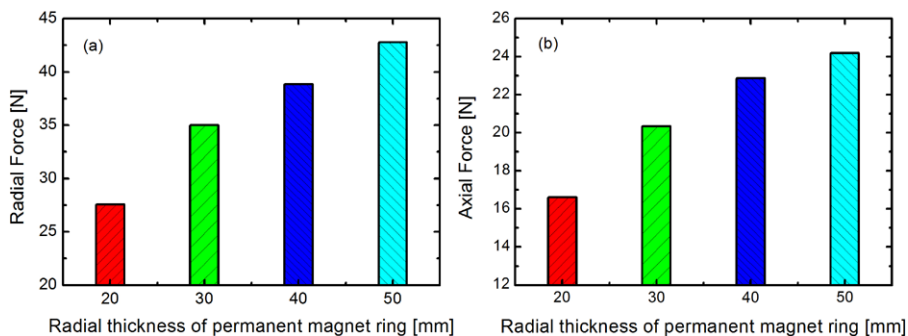


Fig. 4 The dependence of the radial force (a) and the axial force (b) on the radial thickness of the permanent magnet rings used to assemble the magnetic rotor (Color figure online)

can see clearly that, the case with an axial height of 3.0 mm of the FM shim exhibits the highest radial force as well as the highest axial force. This finding implies that, for the configuration of Type III, the optimal performance concerning the radial/axial force can be expected if the sum of the axial height of the PM ring and the FM shim equals to the axial height of HTS bulk.

3.3 The Radial/Axial Force with Different Radial Thickness of the FM Ring

Using the same course as section 3.2 but altering the radial thickness of the PM ring with 3 mm axial height of the FM shim, the dependence of the radial force and the axial force upon this geometrical parameter of the PM ring is investigated and the results are plotted as bar chart in Fig. 4. This figure shows that, the increase of the radial thickness of the PM ring will always enhance the radial force as well as the axial force, but its margin decreases, especially for the case of the axial force. The increase of the radial thickness of the PM ring will shorten the shaft chamber of the magnetic rotor while escalating the cost of the PM ring. Therefore, for a given dimension of the magnetic rotor, the radial thickness of the PM ring requires the task of optimization.

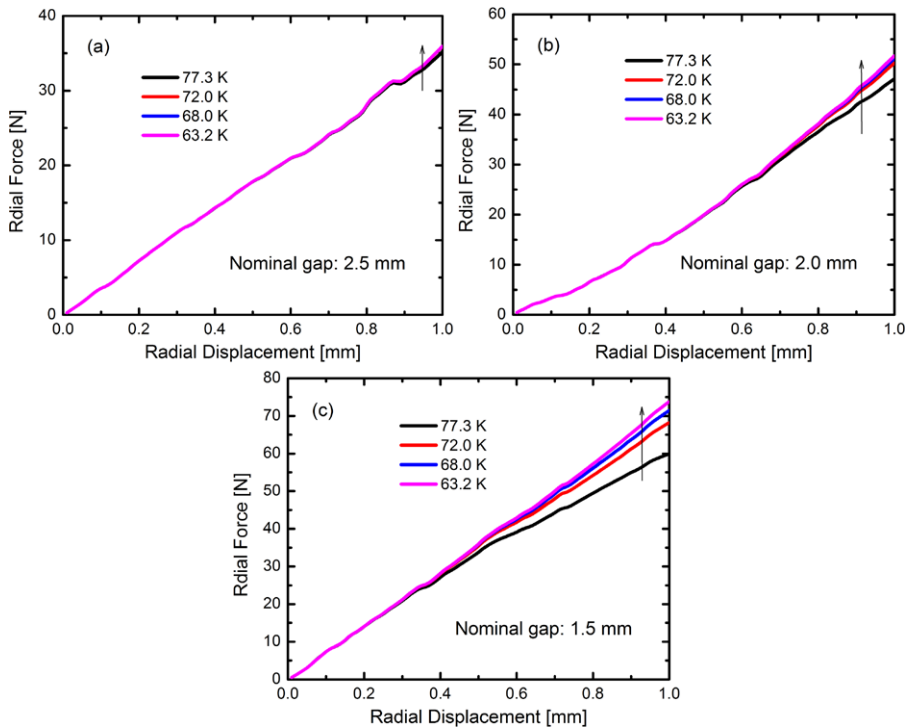


Fig. 5 The calculated radial force exerting on the two symmetric high temperature superconductors during the radial movement relative to a magnetic rotor at different operating temperatures of 77.3, 72.0, 68.0 and 63.2 K. The nominal gap is 2.5 mm for (a), 2.0 mm for (b) and 1.5 mm for (c). The maximum radial displacement is of 1 mm. The operating temperature for each plot decreases with the arrow shown in each figure (Color figure online)

3.4 The Radial/Axial Force at Different Operating Temperatures

With the variation of $j_{c,ab}$ and $j_{c,c}$ and index n in terms of the operating temperature T to obey the proportional relation [21]

$$j_{c,ab}(T) \sim [1 - (T/T_c)^2]^2, \quad \text{and} \quad j_{c,c}(T) \sim [1 - (T/T_c)^2]^2, \quad \text{and} \\ n(T) \sim 1 - (T/T_c)^2$$

we investigated how the radial and axial force vary with the operating temperature at different nominal gaps. Note that the value of $j_{c,ab}$ or of $j_{c,c}$ or of n at other operating temperatures was determined by its value at liquid nitrogen. The index n is actually estimated by $n = U/(\kappa T)$, where the pinning potential U is approximated to be proportional to $1 - (T/T_c)^2$ [21] and κ the Boltzmann constant.

The results at four different operating temperatures, i.e., 77.3, 72.0, 68.0 and 63.2 K, are given in Fig. 5 for the radial force and in Fig. 6 for the axial force. From these figures, one can see that, with the decrease of the nominal gap, the enhancement of both the radial force and axial force at the maximum displacement become

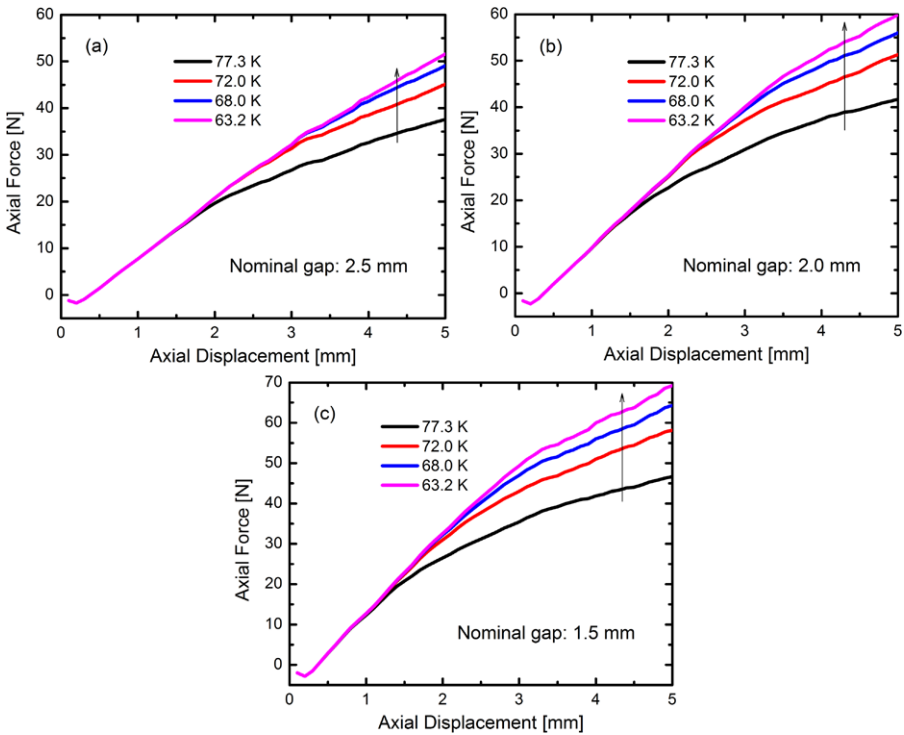


Fig. 6 The calculated axial force exerting on a high temperature superconductor during the axial movement parallel to a magnetic rotor at different operating temperatures of 77.3, 72.0, 68.0 and 63.2 K. The nominal gap is 2.5 mm for (a), 2.0 mm for (b) and 1.5 mm for (c). The maximum axial displacement is of 5 mm. The operating temperature for each plot decreases with the arrow shown in each figure (Color figure online)

more and more noticeable and the displacement where the force curve for a lower operating temperature begins to be higher than the force curve for a higher operating temperature approaches to the initial position. This finding suggests that, despite the decrease of the operating temperature can enhance the critical current density of the HTS, this enhancement of the critical current density cannot lead to a remarkable increase of the radial force and axial force at a large nominal gap such as 2.5 mm in our investigation because the magnetic field to which the HTS bulk exposed is not strong enough to make the best use of the enhanced performance of the HTS due to the decrease of the operating temperature. Therefore, the optimized operating temperature for a HTS bearing is strongly dependent upon the prescribed nominal gap and the magnetic field where the HTS bulks work.

4 Conclusions

We realized a finite-element environment by which the three-dimensional magnetic interaction between the HTS bulk and the magnetic rotor can be investigated. Our

investigation for the purpose of directing the practical design of a HTS bearing in this paper finds that:

The configuration with the axial height of each HTS element in the HTS stator equals to the axial height of the PM ring plus the FM shim and the HTS element to the FM shim centrally (see Fig. 1(d)) shows the best overall performance concerning the radial force as well as the axial force.

The increase of the radial thickness of the PM ring will enhance both the radial force and the axial force, but its margin decreases. Therefore, an optimized value of the radial thickness of the PM ring exists in terms of the volume of the PM ring and the shaft chamber required for mechanical purpose.

Decreasing the operating temperature will enhance the critical current density of the HTS, however, when the nominal gap is not very small, or in other words, the magnetic field where the HTS bulk locates is not very strong, this enhancement of the critical current density cannot lead to a remarkable increase of the radial force as well as the axial force. Therefore, the optimized operating temperature for a HTS bearing is strongly dependent upon the prescribed nominal gap and the magnetic field where the HTS bulks work.

Acknowledgements This work was supported by the National Natural Science Foundation of China (50906093, 51007076), the Fundamental Research Funds for the Central Universities under Grant SWJTU11ZT34, and the Cultivation Foundation for Excellent Doctoral Dissertation of Southwest Jiaotong University. Our great thanks should go to the anonymous reviewers whose suggestions improve the quality of this paper considerably.

References

1. J.R. Hull, *Supercond. Sci. Technol.* **13**, R1 (2000)
2. P. Kummeth, W. Nick, H.W. Neumueller, *Physica C* **426–431**, 739 (2005)
3. Z. Deng, Q. Lin, J. Wang, J. Zheng, G. Ma, Y. Zhang, S. Wang, *Cryogenics* **49**, 259 (2009)
4. B.J. Park, Y.H. Han, S.Y. Jung, C.H. Kim, S.C. Han, J.P. Lee, B.C. Park, T.H. Sung, *Physica C* **470**, 1772 (2010)
5. Q.X. Lin, D.H. Jiang, G.T. Ma, J.S. Wang, Z.G. Deng, J. Zheng, S.Y. Wang, C.Y. Yuan, *IEEE Trans. Appl. Supercond.* **22**, 5201604 (2012)
6. K. Demachi, A. Miura, T. Uchimoto, K. Miya, H. Higawa, R. Takahata, H. Kamenno, *Physica C* **357–360**, 882 (2001)
7. K. Demachi, K. Matsunaga, *Physica C* **412–414**, 789 (2004)
8. Y. Luo, T. Takagi, K. Miya, *Cryogenics* **39**, 331 (1999)
9. R. Shiraishi, K. Demachi, M. Uesaka, *Physica C* **392–396**, 734 (2003)
10. I. Masaie, K. Demachi, T. Ichihara, M. Uesaka, *IEEE Trans. Appl. Supercond.* **15**, 2257 (2005)
11. I. Masaie, K. Demachi, T. Ichihara, M. Uesaka, *IEEE Trans. Appl. Supercond.* **16**, 1807 (2006)
12. N. Koshizuka, *Physica C* **445–448**, 1103 (2006)
13. M. Strasik, J.R. Hull, J.A. Mittleider, J.F. Gonder, P.E. Johnson, K.E. McCrary, C.R. McIver, *Supercond. Sci. Technol.* **23**, 034021 (2010)
14. F.N. Werfel, U. Floegel-Delor, T. Riedel, R. Rothfeld, D. Wippich, B. Goebel, G. Reiner, N. Wehlau, *IEEE Trans. Appl. Supercond.* **20**, 2272 (2010)
15. F.N. Werfel, U. Floegel-Delor, R. Rothfeld, T. Riedel, B. Goebel, D. Wippich, P. Schirrmeister, *Supercond. Sci. Technol.* **25**, 014007 (2012)
16. G.T. Ma, J.S. Wang, S.Y. Wang, *IEEE Trans. Appl. Supercond.* **20**, 2219 (2010)
17. G.T. Ma, H.F. Liu, J.S. Wang, S.Y. Wang, X.C. Lin, J. Supercond. Nov. Magn. **22**, 841 (2009)

18. R. Pecher, M.D. McCulloch, S.J. Chapman, L. Prigozhin, C.M. Elliot, in *EUCAS 2003*, Sorrento, Italy, Sep. 14–18, 2003
19. M. Murakami, T. Oyama, H. Fujimoto, S. Gotoh, K. Yamaguchi, Y. Shiohara, N. Koshizuaka, S. Tanaka, *IEEE Trans. Magn.* **27**, 1479 (1991)
20. G.T. Ma, J.S. Wang, S.Y. Wang, *IEEE Trans. Appl. Supercond.* **20**, 2228 (2010)
21. T. Matsushita, *Flux Pinning in Superconductors* (Springer, Berlin, 2007)